An Efficient Approach to Modeling of Quasi-Planar Structures Using the Formulation of Power Conservation in Spectral Domain

Tongqing Wang and Ke Wu, *Senior Member, IEEE*

***Abstract*—An enhanced spectral domain approach (SDA) is developed for analysis of complex quasi-planar transmission lines. The method is based on a combination of spectral domain formulation and power conservation theorem. The relationship between electric and magnetic fields is established inside dielectric layers by using the conventional SDA while characteristic equation related to interface conditions is derived through the power conservation theorem. Maintaining the inherent advantages of the SDA, this technique is able to easily handle more complex quasi-planar structures. Generalized power formulation is also presented to calculate characteristic impedance. Convergence behavior is discussed considering the nature of power conservation. Various finlines with finite thickness of conductors are analyzed to demonstrate its applications.**

I. Introduction

With ever increasing device density and operating frequency in monolithic and hybrid integrated circuits, electromagnetic modeling of various quasi-planar transmission lines is mandatory in accurately predicting circuit performance and efficiently compressing design cycle. Many analysis methods usually present a compromise between accuracy and efficiency of numerical calculations, which are no longer suitable for growing demand of accurate analysis over wide frequency spectrum up to millimeter-wave range. The development of generalized and rigorous field-theoretical approaches, which are able to consider the effect of finite thickness of metal as well as grooves/pedestals, is therefore pertinent for successful applications. So far, a number of hybrid-mode techniques have been presented for analysis of a class of complex quasi-planar structures, mode-matching method [1], complex power conservation technique [2], transverse resonance technique [3], [4], method of lines [5], modified SDA [6], [7], to name a few examples. It has been recognized that the SDA is the most popular technique today. This is mainly driven by two facts. One is that the Green's function and field quantities are handled in the spectral domain through efficient and simple algebraic algorithm. The other is that Galerkin's technique makes it possible to obtain accurate results with very low determinant order of the characteristic equation. This is usually done through an appropriate choice of basis functions which satisfy the edge singularity of currents on strips or of fields in slots. Its early applications and theoretical framework were reviewed in [8]. Recently, much effort has been made to extend the SDA to modeling of a class of novel and complicated quasi-planar structures. The mixed spectral domain approach was presented in [9], [10] for characterization of suspended planar transmission lines with pedestals and various dielectric-loaded ridge waveguides. The CPW electrodes including conductor thickness have been analyzed in [11] for the Ti:$LiNbO_3$ electrooptic modulator through an extended spectral-domain approach based on integral equations. This approach has been also used to determine the characteristics of planar transmission lines with finite metallization thickness and lossy substrates containing magnetized ferrites in [12], [13]. However, these modified versions of the SDA may suffer from somehow tedious formulations as the complexity of structures increases. The spectral domain and equivalent boundary method [14] was proposed to model generalized coplanar transmission lines embedded in a bianisotropic multilayered medium. Nevertheless, this approach with simple analytical process ignored the effect of finite thickness of conductors.

In this work, a novel enhanced spectral domain approach is proposed to analyze propagation characteristics of a class of complex quasi-planar transmission lines. This technique takes into account the effect of various structural parameters such as finite thickness of conductors and grooves/pedestals while maintaining the advantageous nature of the SDA. It is essentially achieved by an appropriate combination of the conventional SDA formulation with the power conservation theorem. In the spectral domain, tangential magnetic field at boundary apertures of each subregion (homogeneous dielectric layer) can be expressed in terms of its electric counterpart through a characteristic matrix. In the space domain, the boundary conditions at the interfaces are satisfied by imposing power conservation theorem. Compared to the conventional and other modified SDA, the proposed technique is more efficient in view of analytical effort and numerical accuracy. This is done by avoiding usually lengthy derivation of the Green's function matrix for complex structures. In addition, this technique features an independent choice of the truncated spectral term in each subregion. The numerical efficiency is, therefore, highly enhanced in terms of the CPU time and memory space. This is in particular important in the analysis of structures containing a large ratio of the lateral width

Manuscript received January 17, 1994; revised August 18, 1994. This work was supported by Natural Science and Engineering Research Council (NSERC) of Canada.

The authors are with the Groupe de Recherches Avancées en Microondes et en Électronique Spatiale (POLY-GRAMES), Department de Génie Électrique et de Génie Informatique, École Polytechnique, Montréal H3C 3A7, Canada .

IEEE Log Number 9410339.

among adjacent subregions. A generalized power formulation is derived for the impedance calculation. Results for finlines with split-housing and finite thickness of metal strips are presented to demonstrate performance and usefulness of the proposed technique.

II. Theory

A. Characteristic Equation

As shown in Fig. 1(a), a generalized planar structure is composed of an arbitrary number of strips/fins deposited on different interfaces of a multilayer dielectric substrate. The consideration of finite metal thickness as well as housing grooves or box frames is important for millimeter-wave applications [2], [15]. Exact electromagnetic characteristics of such a structure can be symbolically described by the following space-domain integral equation in the frequency domain

$$\vec{E}_t = \iint_s \vec{\vec{G}}(\vec{r}\,|\,\vec{r}\,') \cdot \vec{J}_t(\vec{r}\,')\, ds \tag{1}$$

where $\vec{\vec{G}}$ stands for the dyadic Green's function, and $\vec{E}_t, \vec{J}_t$ are the tangential components of electric fields and current density at interfaces involving strips/fins. In the spectral domain, the convolutional equation (1) is transformed into a simple algebraic equation, such that

$$\tilde{\vec{E}}_t = \tilde{\tilde{\vec{G}}} \cdot \tilde{\vec{J}}_t. \tag{2}$$

The tilde over these quantities indicates the spectral-domain transform. Obviously, the key to apply this approach is to obtain the spectral domain Green's function $\tilde{\tilde{\vec{G}}}$ for a specific structure. So far, a variety of modification and improvement related to the SDA for analysis of planar structures are mainly on derivation of the Green's function. With regard to complex multilayer structures considering finite thickness of metal, grooves and pedestals, the analytical process gets much more involved and may become very difficult as the number of subregions including dielectrics, conductors and grooves/pedestals increases. To solve this bottleneck problem, a novel enhanced SDA is introduced for generalized planar structures. For a concise demonstration of its principle, perfect conductors and isotropic/lossless dielectrics are assumed.

The whole structure is divided into a number of rectangular homogeneous subregions which are interconnected to each other and bounded by lateral conducting walls. The electromagnetic fields in the ith subregion in Fig. 1(b) can be expanded in the spectral domain

$$\begin{pmatrix} \vec{E} \\ \vec{H} \end{pmatrix}^i = \sum_{n=-\infty}^{+\infty} \begin{pmatrix} \tilde{\vec{E}}(y) \\ \tilde{\vec{H}}(y) \end{pmatrix}_n^i \cdot e^{-j(\alpha_n^i \cdot x + \beta \cdot z)} \tag{3}$$

where

$$\begin{pmatrix} \tilde{\vec{E}}(y) \\ \tilde{\vec{H}}(y) \end{pmatrix}_n^i = \frac{1}{a_i} \int_{a_i} \begin{pmatrix} \vec{E} \\ \vec{H} \end{pmatrix}^i \cdot e^{j(\alpha_n^i \cdot x + \beta \cdot z)} \cdot dx \tag{4}$$

with

$$\alpha_n^i = \frac{2n\pi}{a_i}.$$

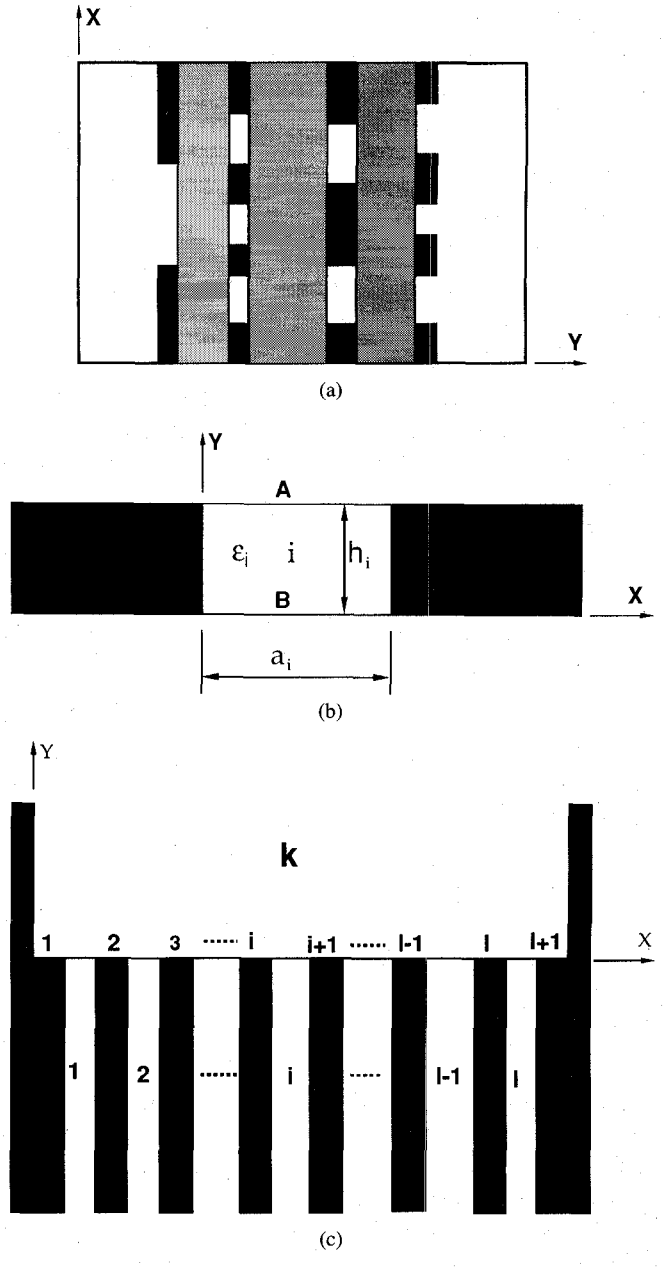

Fig. 1. (a) Cross section of a generalized planar transmission line, (b) any subregion of (a), and (c) any interface of (a).

Substituting (3) into Maxwell's curl equations yields

$$\underbrace{\begin{bmatrix} 0 & \nabla\times \\ \nabla\times & 0 \end{bmatrix}}_{\tilde{\tilde{D}}} \cdot \underbrace{e^{-j(\alpha_n^i \cdot x + \beta \cdot z)} \cdot \begin{pmatrix} \tilde{\vec{E}}(y) \\ \tilde{\vec{H}}(y) \end{pmatrix}_n^i}_{\overline{A}} = j\omega \cdot \underbrace{\begin{bmatrix} \varepsilon & \\ & -\mu_0 \end{bmatrix}^i}_{\tilde{\tilde{M}}} \cdot \overline{A}. \tag{5}$$

In this matrix equation, $\overline{A}$ is a column vector consisting of electric and magnetic fields for the nth spectral component. Using a coordinate transform (rotation) similar to [6], a decoupled equation of the y-directed transverse TE and TM

fields is obtained

$$\frac{d}{dy}\begin{pmatrix} E_u \\ H_v \\ E_v \\ H_u \end{pmatrix}^i = \begin{bmatrix} 0 & j\omega\mu_0 & 0 & 0 \\ \frac{\gamma^2}{j\omega\mu_0} & 0 & 0 & 0 \\ 0 & 0 & 0 & -\frac{\gamma^2}{j\omega\varepsilon} \\ 0 & 0 & -j\omega\varepsilon & 0 \end{bmatrix}_n^i \cdot \begin{pmatrix} E_u \\ H_v \\ E_v \\ H_u \end{pmatrix}_n^i \tag{6}$$

with $\gamma^2 = \alpha^2 + \beta^2 - \omega^2 \cdot \varepsilon \cdot \mu_0$. Note that the relationship between the original and transformed field components is characterized by the coordinate transform. Transmission line solution of (6) leads to two matrix equations which relate aperture fields to each other at lower and upper boundaries, such that

$$\begin{pmatrix} \tilde{H}_x^- \\ -\tilde{H}_z^- \end{pmatrix}_n^i = \frac{1}{j\omega\mu_0\gamma}\begin{bmatrix} \gamma^2-\beta^2 & -\alpha\cdot\beta \\ -\alpha\cdot\beta & \gamma^2-\alpha^2 \end{bmatrix}_n^i \cdot \left\{ \frac{1}{th(\gamma\cdot h)}\begin{pmatrix} \tilde{E}_z^- \\ \tilde{E}_x^- \end{pmatrix} - \frac{1}{sh(\gamma\cdot h)}\begin{pmatrix} \tilde{E}_z^+ \\ \tilde{E}_x^+ \end{pmatrix} \right\}_n^i \tag{7}$$

and

$$\begin{pmatrix} \tilde{H}_x^+ \\ -\tilde{H}_z^+ \end{pmatrix}_n^i = \frac{1}{j\omega\mu_0\gamma}\begin{bmatrix} \gamma^2-\beta^2 & -\alpha\cdot\beta \\ -\alpha\cdot\beta & \gamma^2-\alpha^2 \end{bmatrix}_n^i \cdot \left\{ \frac{1}{sh(\gamma\cdot h)}\begin{pmatrix} \tilde{E}_z^- \\ \tilde{E}_x^- \end{pmatrix} - \frac{1}{th(\gamma\cdot h)}\begin{pmatrix} \tilde{E}_z^+ \\ \tilde{E}_x^+ \end{pmatrix} \right\}_n^i. \tag{8}$$

The superscripts $(-)$ and $(+)$ denote the interfaces at $y = +0$ and $y = h_i - 0$, respectively. Naturally, the tangential components of electric field at the top and bottom metallic ground planes of the shielding box are zero.

In the space domain, the tangential electric and magnetic fields should satisfy the remaining boundary and continuity conditions at the interfaces as illustrated in Fig. 1(c). In view of the interface geometry, these conditions can separately be stated in two different parts

$$\begin{pmatrix} \vec{E}_t^- \\ \vec{H}_t^- \end{pmatrix}^k = \sum_{i=1}^{I}\begin{pmatrix} \vec{E}_t^+ \\ \vec{H}_t^+ \end{pmatrix}^i \quad \text{on apertures}$$

$$\begin{pmatrix} \vec{E}_t^- \\ \vec{H}_t^- \end{pmatrix}^k = \sum_{i=1}^{I+1}\begin{pmatrix} 0 \\ \vec{J}_t^+ \end{pmatrix}^i \quad \text{on conductors} \tag{9}$$

in which the subscript "t" refers to the x-z plane, and "k" is the notation of the region connected to an I-furcated waveguide junction. On the basis of the complementary property between $\vec{E}_t$ and $\vec{J}_t$, the power conservation in the transverse direction should hold, which is determined by the following equation:

$$\int_{a_k} (\vec{E}_t^- \times \vec{H}_t^{-'})^k \, dx = \sum_{i=1}^{I}\int_{a_i} (\vec{E}_t^+ \times \vec{H}_t^{+'})^i \, dx \tag{10}$$

Invoking Parseval theorem, (10) is transformed into the spectral domain such that

$$\frac{1}{a_k}\sum_{n=-\infty}^{+\infty}\begin{pmatrix} \tilde{E}_x^- \cdot \tilde{H}_z^{-*} \\ \tilde{E}_z^- \cdot \tilde{H}_x^{-*} \end{pmatrix}_n^k = \sum_{i=1}^{I}\frac{1}{a_i}\sum_{n=-\infty}^{+\infty}\begin{pmatrix} \tilde{E}_x^+ \cdot \tilde{H}_z^{+*} \\ \tilde{E}_z^+ \cdot \tilde{H}_x^{+*} \end{pmatrix}_n^i. \tag{11}$$

Substituting (7) and (8) into (11), a set of linear homogeneous equations is derived. Propagation constant β can be obtained simply through the application of Galerkin's technique. In numerical calculations, the infinite sum of (11) in the spectral domain is truncated to a finite number. The spectral terms of both sides in (11) may be chosen independently as long as the power conservation is guaranteed. As will be shown in next section, smaller number of spectral terms in subregion with small lateral widths is required to achieve accurate results. This process greatly enhances the numerical efficiency in terms of the CPU time and memory space.

B. Characteristic Impedance

The characteristic impedance is a crucial parameter in computer-aided design of passive and active circuits. In the following, various finlines are considered as examples of analysis. Note that there is no unique definition of impedance in the non-TEM structures in which path integrals of modal fields are arbitrary. On the basis of practical consideration, the voltage-power definition seems to be more appropriate for slot-like structures. Considering the finite thickness of conductors, the two different slot voltages (V_A and V_B) may be obtained which depend on the upper and lower boundary apertures (A and B integral paths in Fig. 1(b), for example). As expected at higher frequencies, the difference between two voltages will be more visible as the thickness increases. Therefore, the average voltage may be defined such that $V_0 = (1/h_i)\cdot\int_0^{h_i}(\int_y E_x \cdot dx)\cdot dy$. This can, in practice, be simplified by assuming a linear variation of V along the y-direction. As a result, V_0 is equal to $(V_A + V_B)/2$.

The total power P is determined by adding up contributions P_i from all partitioned subregions. In the spectral domain, an explicit formulation of P_i can be derived in terms of the field components in the u-v coordinate system

$$P_i = \frac{1}{2a_i}\sum_{n=-\infty}^{+\infty}\underbrace{\begin{pmatrix} \frac{\beta}{\omega\mu_0} & \frac{\omega\varepsilon\beta}{\gamma^2} & \frac{\alpha}{\omega\mu_0} \end{pmatrix}_n^i}_{\overline{C}}\cdot\underbrace{\begin{pmatrix} P_a \\ P_b \\ P_c \end{pmatrix}_n^i}_{\overline{P}} \tag{12}$$

where

$$P_a = (|E_u^-|^2 + |E_u^+|^2)\cdot\frac{sh(2\gamma h)-2\gamma h}{4\gamma\cdot sh^2(\gamma h)} + E_u^-\cdot E_u^+\cdot\frac{\gamma h\cdot[1-sh(\gamma h)]}{sh(\gamma h)\cdot th(\gamma h)}$$

$$P_b = (|E_v^-|^2 + |E_v^+|^2)\cdot\frac{sh(2\gamma h)+2\gamma h}{4\gamma\cdot sh^2(\gamma h)} - E_v^-\cdot E_v^+\cdot\frac{\gamma h\cdot[1+sh(\gamma h)]}{sh(\gamma h)\cdot th(\gamma h)}$$

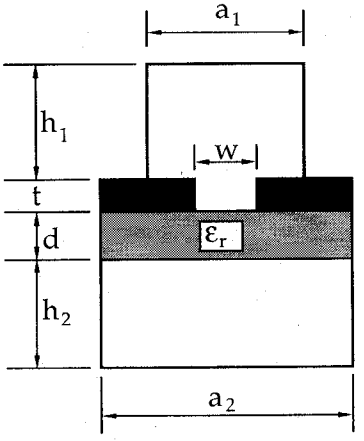

Fig. 2. Structure and dimensions of the asymmetrical finline.

$$P_c = \frac{1}{\gamma \cdot th(\gamma h)} \left(E_u^- \cdot E_v^- + E_u^+ \cdot E_v^+ - (E_u^- \cdot E_v^+ + E_u^+ \cdot E_v^-) \cdot \frac{1}{ch(\gamma h)} \right). \quad (13)$$

In these equations, $E_{u,v}^{+,-}$ are known field quantities defined in the ith subregion, which are directly related to the original fields in the x-z coordinate system through a simple rotation [6]. Obviously, a simple and easy-to-handle formulation is proposed for power calculation that is usually lengthy. This is in particular meaningful in the case of complex multilayer structures considering finite thickness of metals, supporting grooves and pedestals.

C. Numerical Convergence

Prior to showing examples of this new algorithm, it is useful to examine inherent behavior of numerical convergence. The Galerkin's technique requires that unknown tangential electric fields at boundary apertures of the ith subregion be expanded in terms of a complete set of basis functions such that

$$\begin{pmatrix} E_x \\ E_z \end{pmatrix}^i = \begin{pmatrix} \sum_{q=1}^{+\infty} \eta_q \cdot f_q(x) \\ \sum_{s=1}^{+\infty} \zeta_s \cdot g_s(x) \end{pmatrix}^i \quad (14)$$

where η_q and ζ_s are the weighted coefficients to be determined. It is known that a good convergence towards exact results can only be achieved by choosing appropriate basis functions which correctly describe the field singularity at relevant conductor edges. Due to the difference of convergence rate between the expanded basis functions and their Fourier series, the basis functions satisfying the edge conditions should be considered to yield efficient calculation with a low order of matrix equation. In this work, a set of sinusoidal basis functions modified by an edge condition term [16] is used in the analysis. The Fourier transform of the basis functions for the symmetrical case, to name an example, is given by

$$\tilde{f}_q = (-1)^{q-1} \frac{\pi w}{4} \left[J_0\left(\alpha \frac{w}{2} + (q-1)\pi\right) + J_0\left(\alpha \frac{w}{2} - (q-1)\pi\right) \right]$$

TABLE I
COMPARISON OF CALCULATED AND MEASURED FREQUENCY-DEPENDENT RESULTS FOR GUIDED WAVELENGTH OF THE ASYMMETRICAL FINLINE. STRUCTURAL PARAMETERS: $w = 1.25$ mm, $d = 0.254$ mm, $\varepsilon_r = 9.9, a_1 = 4.42$ mm, $a_2 = 6.42$ mm, $t = 0$ mm, $h_1 = 5.41$ mm, $h_2 = 5.16$mm

Freg. (GHz)	λ_g measured	λ_g calculated		
		[15]	[9]	This work
17.6	12.50	12.42	12.37	12.37
18.0	12.09	12.07	12.02	12.02
18.4	11.75	11.73	11.68	11.68
18.8	11.46	11.42	11.37	11.37
19.2	11.18	11.17	11.07	11.07
19.6	10.94	10.83	10.78	10.78
20.0	10.62	10.56	10.51	10.51

$$\tilde{g}_s = (-1)^{s-1} \frac{j\pi w}{4} \left[J_0\left(\alpha \frac{w}{2} + s\pi\right) - J_0\left(\alpha \frac{w}{2} - s\pi\right) \right] \quad (15)$$

with J_0 being the zero-order Bessel function of the first kind. The index n denoting the spectral terms is ignored in (15) for simplicity. The choice of the limiting spectral term for the basis functions mainly depends on the convergence nature of $\tilde{f}_q$. It is easily found that the asymptotic behavior of $\tilde{f}_q$ is in accordance with $\alpha^{-0.5}$ as $n \to \infty$. This suggests that the relative convergence criterion such that $N_k/N_i = C \cdot a_k/a_i$ as already discussed in [15] should be fulfilled for any adjoining subregions in which N_k and N_i are the limiting spectral terms for the basis functions defined in the subregions a_k and a_i, respectively. The coefficient C is then determined by the relative field intensity regarding the relevant adjoining subregions, thereby depending on the structural parameters as well as the spectral terms. The value of C falls usually into the range of 0.2–5.0. C is larger than 1 as a_k/a_i is smaller than 1, for example. In general, the convergence behavior of the propagation constant and characteristic impedance is different with respect to the spectral terms for a given number of the basis functions. This will be discussed subsequently.

III. Numerical Examples

In the following, asymmetrical finlines are analyzed as examples to demonstrate performance and applications of the proposed approach. The basis functions used throughout the paper are truncated at $q = 3$ and $s = 2$, which turn out to be sufficient. To begin with, frequency-dependent characteristics of the finline depicted in Fig. 2 are calculated and shown in Table I. Our results are in excellent agreement with [9], [15], thereby validating the proposed approach. Fig. 3 shows dispersion curves and characteristic impedance of the dominant mode for a bilateral finline with three different thickness of lines. The results for the zero thickness agree well with [16]. The computer program is implemented in a PC486 with 50 MHz clock speed. The CPU time is about 2 seconds per frequency sample.

The effect of the modal voltages (V_A, V_B, V_0) defined at different position across the slot on the characteristic impedance is illustrated in Fig. 4. The results indicate that the relative deviation of characteristic impedance increases linearly with the thickness of conductors. As expected, such an effect is

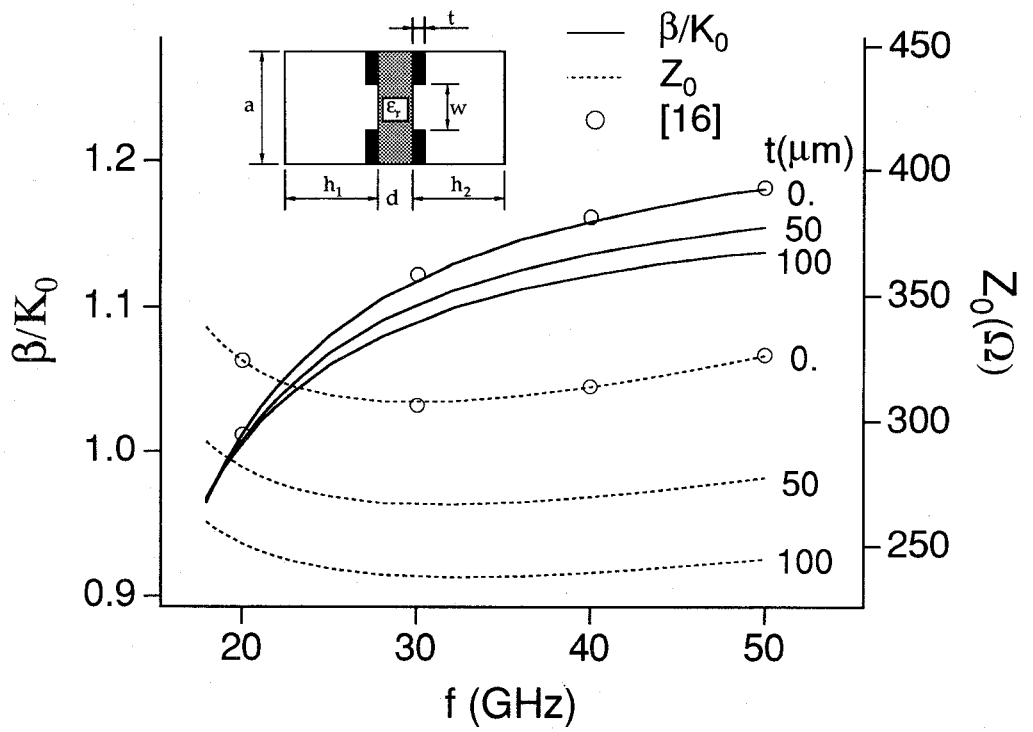

Fig. 3. Dispersion characteristics of the normalized propagation constant and characteristic impedance versus different finite thickness of metallization for a bilateral finline with parameters: $w = 0.3$ mm, $d = 0.125$ mm, ε_r =3.75, $a = 3.556$ mm, $h_1 + t = h_2 + t = 3.4935$ mm.

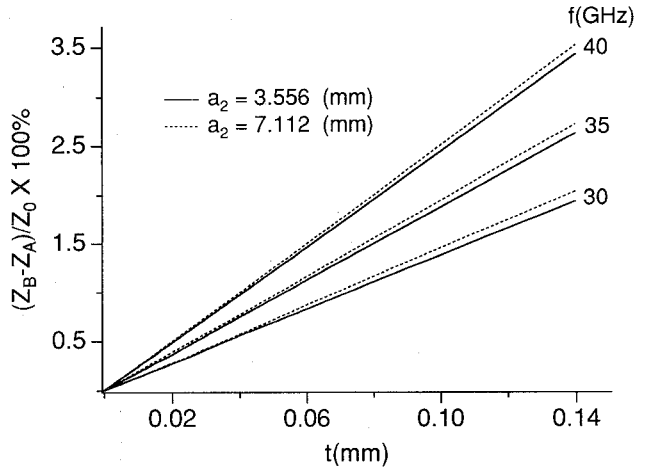

Fig. 4. Relative deviation of the characteristic impedance as a function of the metallization thickness for different definition of voltage in terms of field path integral in the finline (see Fig. 2). $w = 0.2$ mm, $d = 0.254$ mm, $\varepsilon_r = 3.75$, $a_1 = 3.556$ mm, $h_1 = h_2 + t = 3.431$ mm.

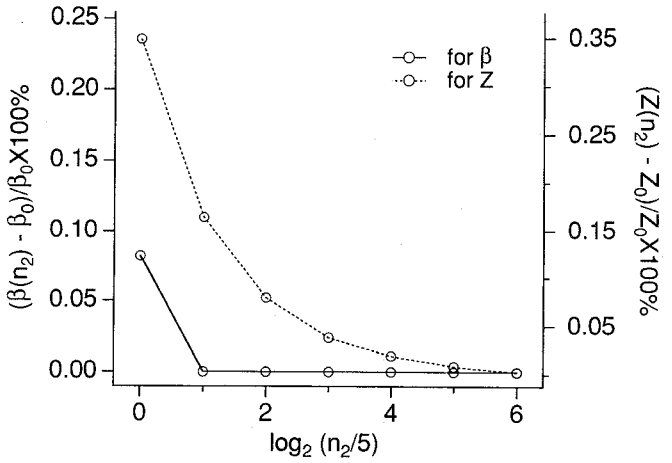

Fig. 5. Convergence behavior of the propagation constant and characteristic impedance versus the limiting number of spectral terms n_2 in Fig. 2 with $w = 0.4$ mm, $d = 0.254$ mm, $\varepsilon_r = 3.75$, $a_1 = 3.556$ mm, a_2 =7.112 mm, $t = 0.1$ mm, $h_1 = h_2 + t = 3.431$mm, $f = 35$ GHz.

more pronounced at higher frequencies. Obviously, the difference of modal voltages is attributed to the integral path over different intensity of electric field across the slot with finite thickness. On the other hand, the difference in convergence behavior between the propagation constant and characteristic impedance is exhibited in Fig. 5 for the asymmetrical finline (see Fig. 2). The number of spectral terms in subregions other than "t" is set to be 600, while the reference values of β_0 and Z_0 is obtained as $n_2 = 600$. It is observed that the convergence rate of β_0 is more rapid as a function of the spectral term than that of Z_0. This indicates that power spectrum are widely spread over a large range of terms. The slow convergence of power calculation compared to the dispersion analysis may be explained by involving the "double" field singularity such as $E_x \times H_y$. Nevertheless, Fig. 5 suggests that sufficiently accurate results are obtained for the given structure as n_2 exceeds 40.

Fig. 6 presents dispersion characteristics including the first higher-order mode and characteristic impedance by considering the effect of finite metallization thickness. It is shown that the influence of the finite thickness is significant on the characteristic impedance over the frequency band of interest.

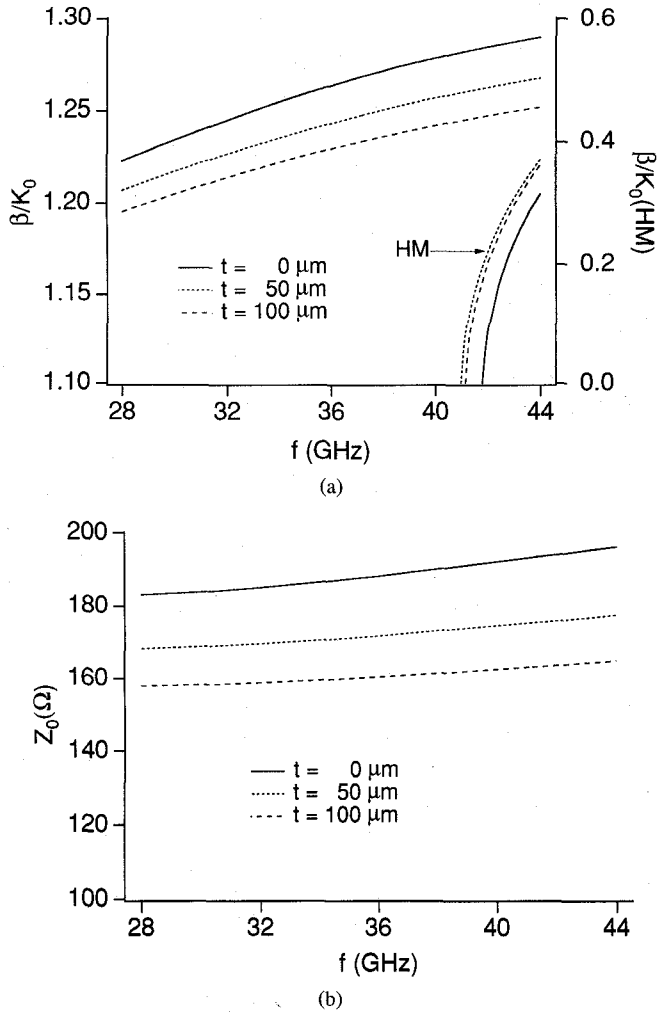

Fig. 6. Dispersion characteristics for different thickness of metallization of the asymmetrical finline (see Fig. 2) with $w = 0.4$ mm, $d = 0.254$ mm, $\varepsilon_r = 3.75$, $a_1 = 3.556$ mm, $a_2 = 7.112$ mm, $h_1 = h_2 + t = 3.431$ mm (HM refers to the first higher-order mode). (a) Normalized propagation constant. (b) Characteristic impedance.

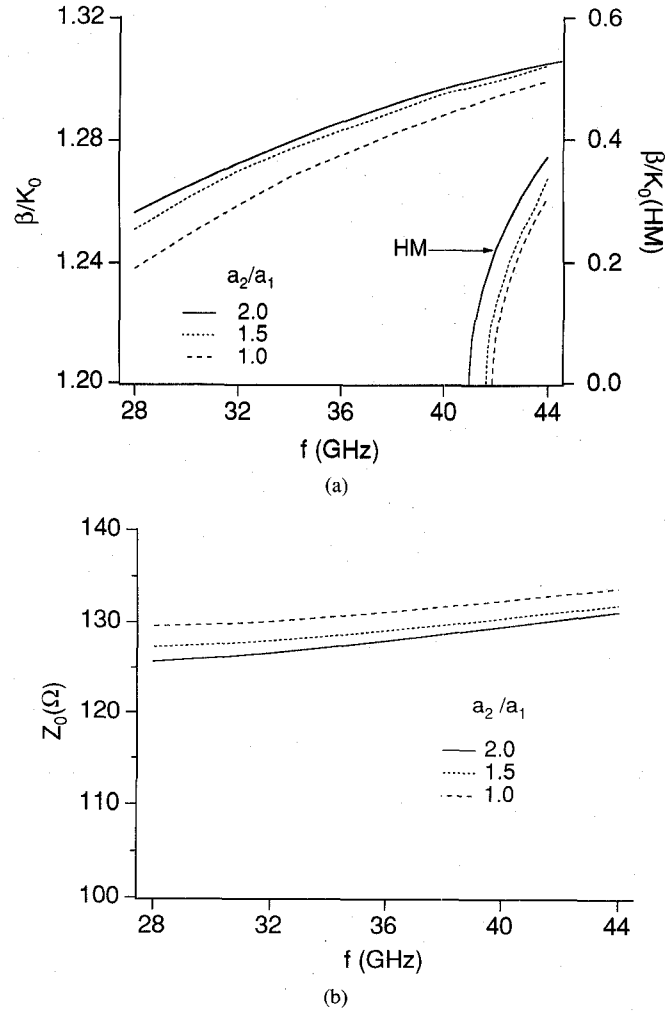

Fig. 7. Frequency-dependent characteristics for different dimension ratio a_2/a_1 described in the asymmetrical finline (see Fig. 2) with $w = 0.2$ mm, $d = 0.254$ mm, $\varepsilon_r = 3.75$, $a_1 = 3.556$ mm, $t = 0.05$ mm, $h_1 = h_2 + t = 3.431$ mm. (HM refers to the first higher-order mode). (a) Normalized propagation constant. (b) Characteristic impedance.

Increasing the metallization thickness decreases the propagation constant and characteristic impedance of the dominant mode. However, the cutoff frequency of the first higher-order mode in the case of $t = 100$ μm moves slightly upwards compared to the case of $t = 50$ μm. This may stem from an opposite field perturbation in y-direction by the separation of housing and concerned metallization thickness. The dispersion curves and characteristic impedance are plotted in Fig. 7 for different housing separation (or contrast of the shielding). In this case, the results considering the effect of finite thickness display similar dispersion characteristics as in [15] for the situation of vanishing thickness. The increase in the housing separation pulls downwards the cutoff frequency of the first higher-order mode for the given structure. Shown in Fig. 8 are the dispersion and characteristic impedance of the even- and odd-modes against different slot widths for a coupled asymmetrical finline with finite thickness. Of course, In contrast to the odd-mode, nearly dispersionless characteristics are observed for the even-mode (quasi-TEM mode) over the frequency of interest.

IV. Conclusion

A novel strategy of using the spectral-domain approach called the enhanced SDA is proposed for accurate theoretical characterization of generalized planar multilayer and multiconductor structures. The approach is formulated by combining the conventional SDA in homogeneous zones and the power conservation theorem at interfaces of different zones. The principal features of the proposed approach are to simplify the derivation of Green's function and extend the inherent advantages of the existing SDA into handling practical complex structures considering finite metallization thickness, housing grooves/separation, and pedestals. The algorithm is easily implemented on a personal computer. A unified yet easy-to-use power formulation is also derived to determine the characteristic impedance for design consideration. The work features a study on convergence characteristics of the propagation constant and impedance. With the power conservation, the limiting number of spectral terms in each subregions can be chosen independently, thereby providing the possibility of

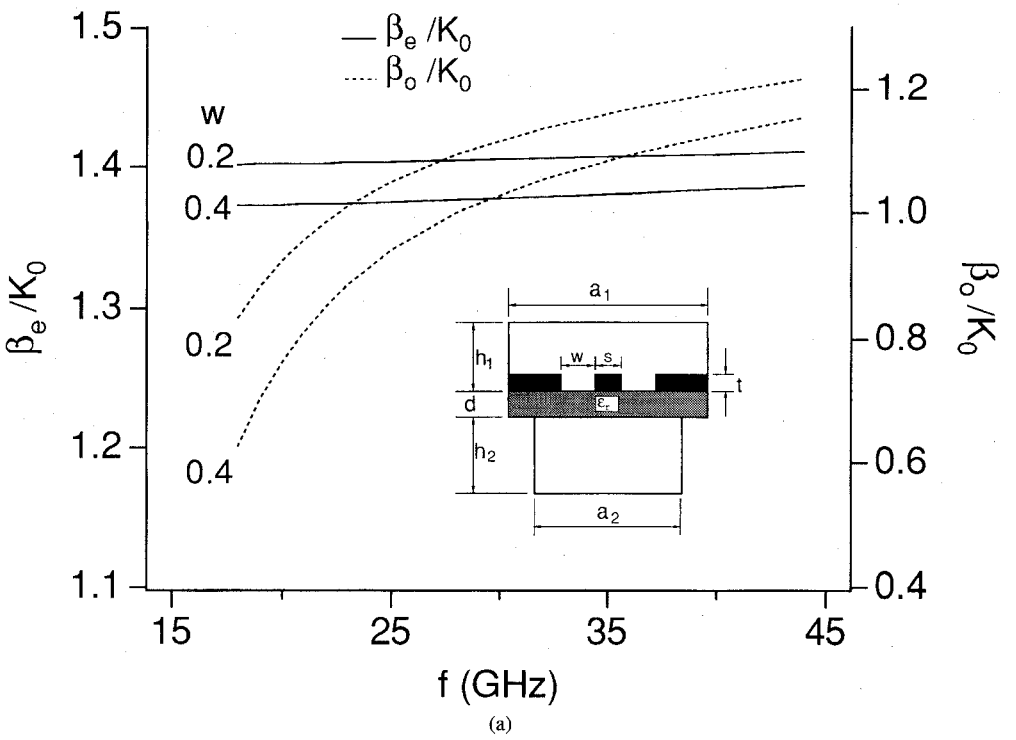

(a)

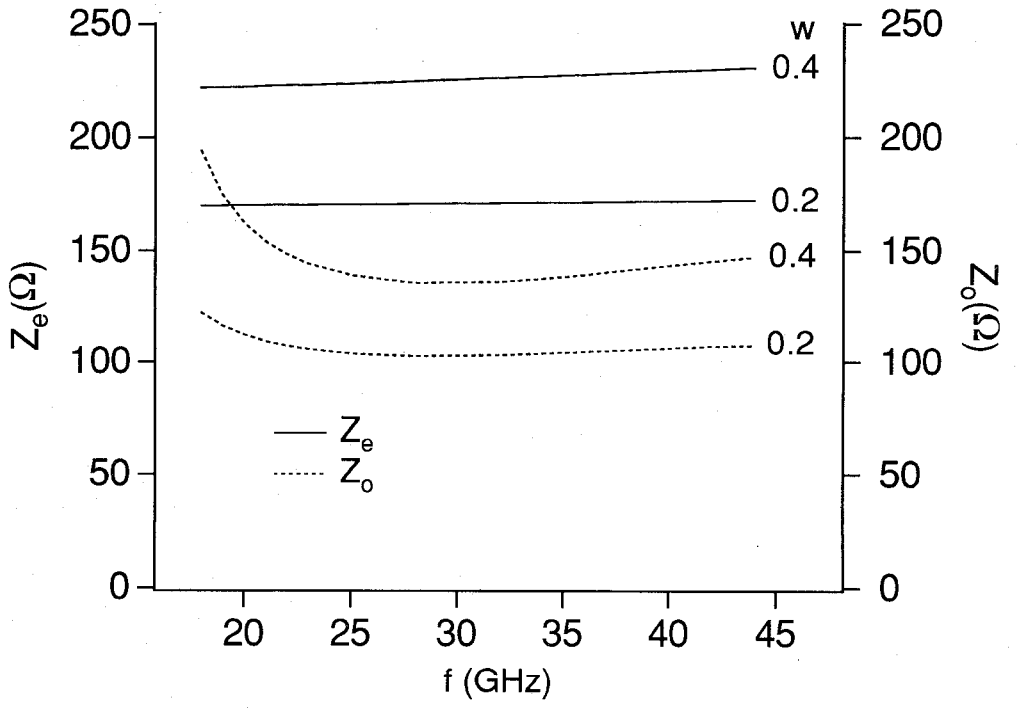

(b)

Fig. 8. Dispersion characteristics of an asymmetrical coupled finline for different slotwidth with $d = 0.254$ mm, $\varepsilon_r = 3.75$, $a_1 = 3.556$ mm, $a_2 = 2$ mm, $t = 0.05$ mm, $h_1 = h_2 = 3.431$ mm, $s = 0.2$ mm (the letters "e" and "o" denote the even mode and the odd mode, respectively). (a) Normalized propagation constant. (b) Characteristic impedance.

reducing drastically calculation expense in terms of memory size and CPU time. Applications of the validated method are demonstrated through calculation and analysis of various asymmetrical finlines. It is believed that the proposed approach can find applications in CAD of a wide range of quasi-planar circuits.

REFERENCES

[1] A. Beyer, "Analysis of the characteristics of an earthed fin line," *IEEE Trans. Microwave Theory Tech.*, vol. MTT-29, pp. 676–680, July 1981.

[2] R. R. Mansour and R. H. Macphie "A unified hybrid-mode analysis for planar transmission lines with multilayer isotropic/anisotropic substrates," *IEEE Trans. Microwave Theory Tech.*, vol. MTT-35, pp.

1382–1391, Dec. 1987.
[3] J. Bornemann and F. Arndt, "Calculating the characteristic impedance of finlines by transverse resonance method," *IEEE Trans. Microwave Theory Tech.*, vol. MTT-34, pp. 85–92, Jan. 1986.
[4] J. Bornemann, "A Scattering-type transverse resonance technique for the calculation of (M)MIC transmission line characteristics," *IEEE Trans. Microwave Theory Tech.*, vol. 39, pp. 2083–2088, Dec. 1991.
[5] Uwe Schulz and R. Pregla,"A new technique for the analysis of the dispersion characteristics of planar waveguides," *AEU*, band 34, helt 4, pp. 169–173, 1980.
[6] T. Itoh, "Spectral domain immitance approach for dispersion characteristics of generalized printed transmission lines," *IEEE Trans. Microwave Theory Tech.*, vol. MTT-28, pp. 733–736, July 1980.
[7] C. M. Krowne, "Fourier transformed matrix method of finding propagation characteristics of complex anisotropic layered media," *IEEE Trans. Microwave Theory Tech.*, vol. MTT-32, pp. 1617–1625, Dec. 1984.
[8] R. H. Jansen, "The spectral-domain approach for microwave integrated circuits," *IEEE Trans. Microwave Theory Tech.*, vol. MTT-33, pp. 1043–1056, Oct. 1985.
[9] C. H. Chan, K. T. Ng, and A. B. Kouki, "A mixed spectral-domain approach for dispersion analysis of suspended planar transmission lines with pedestals," *IEEE Trans. Microwave Theory Tech.*, vol. 37, pp. 1716–1723, Nov. 1989.
[10] K. T. Ng and C. H. Chan, "Unified solution of various dielectric-loaded ridge waveguides with a mixed spectral-domain method," *IEEE Trans. Microwave Theory Tech.*, vol. 37, pp. 2080–2085, Dec. 1989.
[11] T. Kitazawa, D. Polifko, and H. Ogawa, "Analysis of CPW for $LiNbO_3$ optical modulator by extended spectral-domain approach," *IEEE Microwave and Guided Wave Letters*, vol. 2, no. 8, pp. 313–315, Aug. 1992.
[12] T. Kitazawa *et al.*, "Planar transmission lines with finitely thick conductors and loss substrates," in *IEEE MTT-S Dig.*, 1991, pp. 769–772.
[13] T. Kitazawa, "Analysis of shielded striplines and finlines with finite metallization thickness containing magnetized ferrites," *IEEE Trans. Microwave Theory Tech.*, vol. 39, pp. pp. 70–74, Jan. 1991.
[14] F. L. Mesa, R. Marqués, and M. Horno, "A general algorithm for computing the bidimensional spectral Green's dyad in multilayered complex bianisotropic media: The equivalent boundary method," *IEEE Trans. Microwave Theory Tech.*, vol. 39, pp. 1640–1649, Sept. 1991.
[15] P. Espes, P. F. Combes, J.-M. Goutoule, and B. Theron, "Asymmetrical finline for space applications using millimeter waves," *IEEE Trans. Microwave Theory Tech.*, vol. 37, pp. 289–298, Feb. 1989.
[16] L. P. Schmidt and T. Itoh, "Spectral domain analysis of dominant and higher order modes in fin-lines," *IEEE Trans. Microwave Theory Tech.*, vol. MTT-28, pp. 981–985, Sept. 1980.

Tongqing Wang, for photograph and biography, please see p. 1114 of this issue of this TRANSACTIONS.

Ke Wu (M'87–SM'92), for photograph and biography, please see p. 1114 of this issue of this TRANSACTIONS.